Volume 20, No 2 | International Journal of Radiation Research, April 2022

A preliminary application research of dual-energy spectral CT in breast cancer diagnosis

L.J. Chen[1], B. Wang[2], S.F. Wang[2], Z.L. Xu[2], L.Z. Jin[2], M.H. Hu[2], G.Y. Wang[2*], X.P. Yang[2*]

[1]Department of Radiology, Lanzhou University Second Hospital, Lanzhou 730030, PR China
[2]Department of Radiology, Taizhou Central Hospital (Taizhou University Hospital), Taizhou 318000, PR China

► ***Original article***

Corresponding authors:
Dr. Xiao-Ping Yang,
Dr. Guo-Yu Wang
E-mail:
lwyxp_zxl@sohu.com,
hswangguoyu@163.com

Received: January 2021
Final revised: August 2021
Accepted: September 2021

Int. J. Radiat. Res., April 2022; 20(2): 283-289

DOI: 10.52547/ijrr.20.2.5

Keywords: *Spectral CT, Breast cancer, Metastatic lymph nodes.*

ABSTRACT

***Background*:** The objective of this study was to retrospectively analyze the application of dual-energy spectral computerized tomography (DECT) to accurately diagnose breast cancer and lymph node metastasis. ***Materials and Methods*:** Between May 2018 and December 2019, 37 patients (22 with breast cancer and 15 with normal breast cancer) who underwent spectral CT imaging were analyzed. Metastatic lymph nodes were identified in 14 patients with breast cancer. Twelve patients who underwent traditional CT were included randomly as the control group to compare the radiation dose with spectral CT. Monochromatic levels with an optimal contrast-to-noise ratio for normal breast tissue were obtained. Quantitative parameters of spectral CT were compared between normal breast and breast cancer patients. The spectral curve, histogram, and scatter plot features of metastatic lymph nodes and primary lesions were analyzed. ***Results*:** The monochromatic level with the optimal contrast-to-noise ratio of the breast was approximately 65keV. All quantitative parameters, including values at 40keV–140keV, the concentrations of iodine, spectral curve slope (λ_{HU}), and relative iodine concentration were increased in breast cancer compared to those in healthy breasts. Metastatic lymph nodes were more consistent with primary breast cancer lesions in the spectral curve, histogram, and scatter plot, especially in the venous phase. Additionally, the radiation of spectral CT was decreased compared to that of traditional CT. ***Conclusion*:** Spectral CT can be used to identify breast cancer and metastatic lymph nodes.

INTRODUCTION

Breast tumors are the most prevalent type of cancer in women across different countries, and their mortality rate ranks first among female malignant tumors [1]. Early detection of lesions and diagnosis of axillary lymph node metastasis is crucial to improve the survival rates of these patients. For breast cancer, contrast-enhanced computerized tomography (CT) imaging of the thorax is used to assess metastases in the lungs, bones, and lymph nodes [2]. However, conventional CT imaging has limited value in accurately evaluating the features of primary breast lesions because of the higher radiation dose, poor resolution when analyzing soft tissues, single imaging, and being subject to the interpretation of the operator [3].

Spectral CT using the gemstone spectral imaging mode is a new imaging method that can achieve high-resolution imaging and material decomposition through the fast switching of tube voltage between 80 kVp and 140 kVp. This can be used for both qualitative and quantitative analyses [4], and when compared with conventional CT imaging, it has obvious advantages. Currently, several numerical parameters of spectral CT have been shown to be relevant for the identification and staging of several types of cancers, such as head, lung, liver, and kidney [5-9]. These parameters include the relative effective atomic number, CT values at 40keV–140keV, spectral curve slope (λ_{HU}), concentration of iodine (IC), and normalized iodine concentration (NIC). A recent study showed that spectral CT is useful for identifying incidental breast lesions, and the results showed that low keV images were valuable for the identification of lesions suggestive of breast cancer, and that tumors exhibited higher levels of IC than healthy tissues from the breast and pectoral muscles [10].

The purpose of our study was to explore whether quantitative parameters from spectral CT could be helpful in the evaluation of cancerous breast tissue and detection of metastasis to lymph nodes. This procedure can potentially improve the limitations of traditional CT when diagnosing primary breast cancer and provide more reliable information for physicians. Few studies have specifically investigated the diagnostic performance of DECT in the characterization of breast disease.

[Downloaded from ijrr.com on 2026-11-12]

[DOI: 10.52547/ijrr.20.2.5]

MATERIALS AND METHODS

Patients

Thirty-seven patients (women, aged 27–69 years; mean age, 47.68 ± 11.04 years) who underwent preoperative chest CT using the GSI mode from May 2018 to December 2019 were enrolled. All patients signed informed consent forms prior to the scan. Fifteen had normal breast density, as confirmed by other imaging techniques and case history. These patients underwent plain and dual-phase contrast-enhanced CT mainly because of other chest diseases (nine mediastinal lesions and six lung lesions). The other 22 patients, who were evaluated retrospectively, were diagnosed with breast cancer after biopsy and histopathological examination; they underwent spectral CT for the screening of metastases to the lungs. There were 20 invasive ductal carcinomas, one invasive lobular carcinoma, and one invasive papillary carcinoma. Metastatic lymph nodes were found in 14 breast cancer patients, 13 of which involved the ipsilateral axillary lymph nodes and 1 involved an interpectoral lymph node. Twelve female patients who underwent dual-phase contrast-enhanced scans with traditional CT were randomly selected as the control group to compare the radiation dose with spectral CT.

CT examination

Before the examination, all patients were required to remove their undergarments and undergo spectral CT (Discovery CT750 HD, GE Healthcare) scans in the supine position, using a scanning range from the thorax entrance to 2 cm below the rib arch. We used the following parameters for spectral CT scans: tube voltage fast-switching (80 kVp to 140 kVp) (cycles of 0.5 ms), 275 mA, 1.25 slice thickness, and a pitch of 1.375. Patients were injected with 1.0 mL/kg nonionic contrast media (Visipaque, 320 mgI/ml, GE Healthcare) using a double-syringe power injector (Bayer, Germany) at 3.0 mL/s. The arterial phase began at 30 s, while the venous phase began 70 s after contrast injection.

Analysis of images

Monochromatic images built from the data of the original scans were analyzed in a dedicated workstation (Advantage Workstation 4.6, GE Healthcare).

Normal breast tissue

The region of interest (ROI) was an area of approximately 25 mm^2 placed in dense areas of normal breast glands on monochromatic images. Monochromatic levels that showed normal breast tissue with an optimal contrast-to-noise ratio (CNR) in plain, as well as dual-phase CT, were obtained using the optimal CNR monochromatic curve, with adipose tissue around the gland tissue in the background. Quantitative parameters were obtained in the plain and dual-phase, including values between 40keV and 140keV, and the spectral curve slope was derived from the formula: λ_{HU} = [CT_{number} (40keV) - CT_{number} (70keV)]/30, IC, and NIC, which was calculated as the IC of normal glands divided by the aorta IC at the same level. The NIC was used to prevent errors caused by different blood flow rates, volumes, or other individual factors. To prevent measurement errors, three ROIs were selected for every scan, and the mean of the three replicate ROIs was used for statistical analysis.

Detection of cancerous breast tissue and metastasis to lymph nodes

Solid levels of homogenous enhancement of cancerous breast tissue and metastatic lymph nodes at their maximum levels were selected. The ROI, in the range of 50%–70% of the parenchyma of the lesion, was positioned in the middle of the lesion, and necrotic tissue, fat, calcification, and blood vessels were avoided. The same ROI was selected on the contralateral normal breast as a comparison group using the same method. CT values between 40keV and 140keV, λ_{HU}, IC, and NIC were measured. The spectral curve, histogram, and scatter plot of the metastatic lymph nodes, together with the primary lesion, were obtained with dual-phase scanning.

Evaluation of the radiation dose

The radiation dose parameters of dual-energy spectral CT and traditional CT with dual-phase contrast-enhanced scanning were recorded. These included the CT dose index volume, dose length product (DLP), and effective dose (ED). The ED was obtained after multiplying the DLP by 0.014, as in the formula ED = DLP × k (where k = 0.014).

Statistical analysis

SPSS version 19.0 was used to analyze the data. Numerical data are presented as mean ± standard deviation (x ± s) and 95% confidence interval (CI). One-way ANOVA was performed to analyze the curve slopes of the normal breast tissue in the plain, arterial, and venous phases. Comparison of spectral parameters from breast cancers and healthy tissues, as well as comparisons of the radiation dose of both spectral and traditional CT, were performed with an unpaired *t*-test. Statistical significance was set at $P < 0.05$.

RESULTS

Normal breast spectral features

The spectral parameters for normal breast tissue in plain and dual-phase CT are listed in table 1. The average monochromatic level that showed normal breast tissue with an optimal CNR in plain, arterial,

[Downloaded from ijrr.com on 2026-11-12]

[DOI: 10.52547/ijrr.20.2.5]

and venous phase scans was approximately 65keV (figure 1). For normal breast tissue, the CT values of 40–140keV in both venous and arterial phases were increased when compared to those with plain CT, especially in the venous phase. Normal glands had enhanced IC and NIC in the venous phase compared to the values obtained in the arterial phase. The X-ray attenuation degree at 40–70keV for normal breast tissue in the plain, arterial, and venous phases was more obvious than other higher keV levels in the spectral curve, and the curve flattened at 70–140keV (figure 2). The curve slopes of normal breast tissue in the plain, arterial, and venous phases were similar, since no statistical difference was detected (F=1.259, P>0.05) (table 2).

Breast cancer spectral features

CT values at 40–140keV, IC, and NIC of both healthy and cancer tissues are listed in tables 3 and 4. These parameters were increased in cancerous breast tissue when compared to healthy tissues, especially in the venous phase *(*p<0.05). The spectral curves are shown in figure 3. For breast cancer, the spectral curve trend was steeper at 40–70keV than for normal breast tissue and then slowed down gradually to 40–140keV in both healthy and cancerous tissues. We detected statistically significant differences in the curve slopes at 40–70keV between healthy and cancerous tissues. By comparing the IC, NIC, and CT values in the arterial and venous phases of breast cancer, we observed that the differences in the IC and NIC were more significant than the differences in CT values. Additionally, we found that the difference in the NIC was more significant than the difference in IC in breast cancer in both phases (figures 4a–4c).

Metastatic lymph node spectral features

The spectral curve, histogram, and scatter plot of cancerous breast tissue and lymph nodes with metastasis were obtained in the arterial and venous phases (figures 5 and 6). As the figures show, the spectral curve, histogram, and scatter plot of the metastatic lymph nodes had different characteristics in both phases compared with primary breast cancer lesions. Metastatic lymph nodes had similar or the same morphological characteristics as the primary breast cancer lesions in the spectral curve, histogram, and scatter plot in the venous phase, while they were different or crossed in the arterial phase. This indicated that the spectral curve, histogram, and scatter plot of the cancerous tissue and metastatic lymph nodes were more consistent in the venous phase; therefore, it would be more accurate to diagnose metastatic lymph nodes when analyzing images in the venous phase.

Radiation dose comparison

The radiation dose comparisons between spectral CT and traditional dual-phase CT are listed in table 5. Both spectral and dual-phase CTs had a lower radiation dose than the traditional CT (P<0.05).

Table 1. Spectral parameters of normal breast tissue.

Items	Plain		Arterial phase		Venous phase	
	`x±s	95% CI	`x±s	95% CI	`x±s	95% CI
Optimal keV	65.55±0.82	(65.2,65.95)	65.70±0.80	(65.35,66.05)	65.80±0.69	(65.50,66.10)
40keV (HU)	33.17±6.60	(28.52,37.89)	41.5±16.95	(36.86,46.25)	50.06±13.94	(46.02,54.11)
50keV (HU)	30.22±2.86	(28.22,32,29)	40.1±11.37	(36.88,43.30)	45.86±9.70	(43.06,48.73)
60keV (HU)	25.81±1.56	(24.70,26.92)	35.05±8.30	(32.59,37.57)	38.68±7.20	(36.58,40.67)
70keV (HU)	24.03±1.58	(22.85,25.21)	33.60±6.98	(31.62,35.67)	36.32±6.61	(34,47,38.18)
80keV (HU)	25.22±3.19	(22.93,27.70)	36.39±6.92	(34.42,38.39)	38.68±6.50	(36.87,40.64)
90keV (HU)	26.07±3.10	(23.84,28.51)	38.16±6.62	(36.21,40.09)	39.93±6.08	(38.23,41.77)
100keV (HU)	25.72±3.50	(23.22,28.44)	38.01±6.63	(35.94,39.93)	39.45±6.05	(37.81,41.32)
110keV (HU)	25.50±3.78	(22.85,28.44)	37.90±6.67	(35.82,39.80)	39.12±6.06	(37.47,41.02)
120keV (HU)	25.32±4.00	(22.56,28.40)	37.81±6.74	(35.66,39.73)	38.88±6.08	(37.22,40.78)
130keV (HU)	25.20±4.16	(22.34,28.40)	37.76±6.80	(35.60,39.70)	38.71±6.11	(37.04,40.64)
140keV (HU)	25.00±4.27	(22.15,28.38)	37.72±6.84	(35.54,39.65)	38.56±6.13	(36.89,40.49)
IC (mg/cc)	-	-	1.42±0.30	(1.13,1.72)	2.10±0.40	(1.63,2.62)
NIC			0.02±0.003	(0.01,0.03)	0.06±0.005	(0.05,0.08)

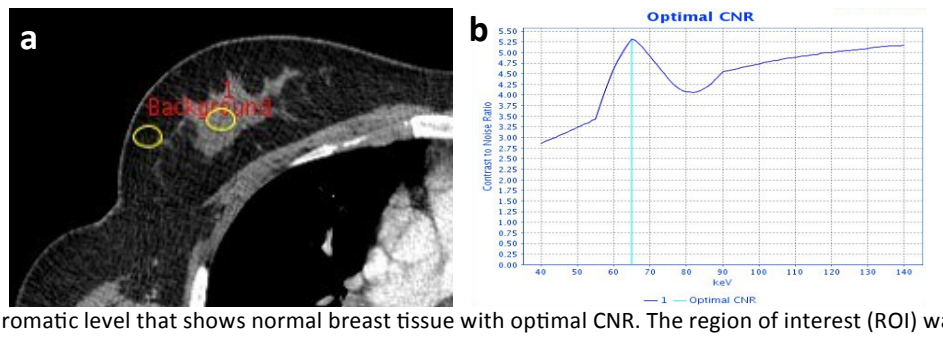


Figure 1. Monochromatic level that shows normal breast tissue with optimal CNR. The region of interest (ROI) was positioned at dense areas of normal breast glands with adipose tissue in the background **(a)**. The ideal contrast-to-noise ratio (CNR) monochromatic curve shows that the monochromatic level that shows normal breast with the optimal CNR is 65keV **(b)**.

[Downloaded from ijrr.com on 2026-11-12]

[DOI: 10.52547/ijrr.20.2.5]

Table 3. The comparison of CT values between breast cancer and normal breast in arterial and venous.

		Arterial phase			Venous phase		
		CT Values (HU)	*t*	*p*-Value	CT Values (HU)	*t*	*P*-Value
Cancer	40keV	114.7±20.31	11.526	0.000	158.15±25.30	17.339	0.000
Healthy		44.33±12.28			51.25±10.76		
Cancer	50keV	90.06±19.37	12.084	0.000	117.93±21.68	17.340	0.000
Healthy		42.56±9.02			46.99±10.10		
Cancer	60keV	69.33±12.31	12.043	0.000	88.28±14.35	17.344	0.000
Healthy		36.76±8.01			39.67±8.00		
Cancer	70keV	58.74±8.86	11.544	0.000	71.50±11.69	14.516	0.000
Healthy		35.25±7.38			37.27±7.27		
Cancer	80keV	56.80±7.48	10.219	0.000	65.27±10.71	11.564	0.000
Healthy		38.31±7.09			39.70±7.14		
Cancer	90keV	55.44±6.64	9.239	0.000	61.51±9.53	10.275	0.000
Healthy		40.02±6.87			40.98±6.62		
Cancer	100keV	52.65±6.25	7.879	0.000	56.99±9.25	8.430	0.000
Healthy		39.85±6.92			40.50±6.54		
Cancer	110keV	50.69±6.14	6.782	0.000	53.81±9.26	6.999	0.000
Healthy		39.70±7.01			40.16±6.52		
Cancer	120keV	49.31±6.14	5.945	0.000	51.56±9.27	5.962	0.000
Healthy		39.59±7.13			39.93±6.50		
Cancer	130keV	48.27±6.18	5.297	0.000	49.83±9.35	5.136	0.000
Healthy		39.53±7.21			39.75±6.52		
Cancer	140keV	47.41±6.23	4.774	0.000	48.48±9.42	4.503	0.000
Healthy		39.47±7.28			39.60±6.51		

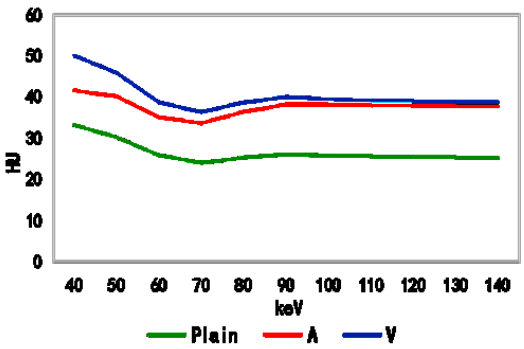


Figure 2. Spectral curves of normal breast tissue in plain, arterial **(A)**, and venous **(V)** phases.

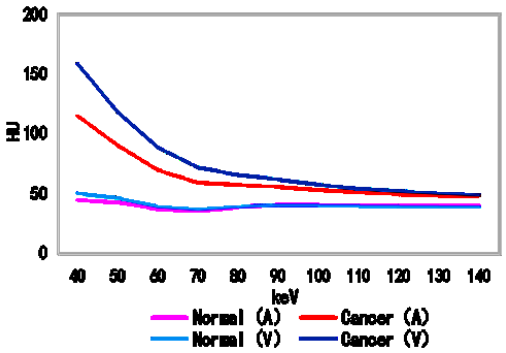


Figure 3. Spectral curves of breast cancer and normal breast tissue in the arterial **(A)** and venous **(V)** Phases.

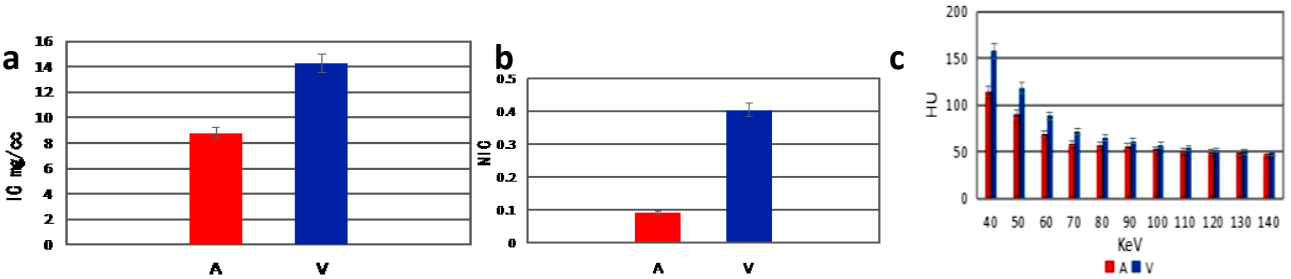


Figure 4. Comparison of iodine concentration (IC) of breast cancer in the arterial **(A)** and venous **(V)** phases **(a)**. Comparison of normalized iodine concentration (NIC) of breast cancer in the A and V phases **(b)**. Comparison of CT values of breast cancer in the A and V phases **(c)**.

Table 2. Comparison of spectral curve slopes for normal breast tissue in the plain, arterial, and venous phases.

λ_{HU}	`x±s	F	*p*-Value
Plain	0.46±0.07		
Arterial phase	0.45±0.05	1.259	> 0.05
Venous phase	0.52±0.08		

Table 4. Comparison of iodine quantification and spectral curve slopes between breast cancer and normal breast tissue in the arterial and venous phases.

Groups		Arterial phase			Venous phase		
		`x±s	*t*	*p*-Value	`x±s	*t*	*p*-Value
Cancer	IC	8.79±1.20	10.465	0.000	14.28±2.37	15.844	0.000
Healthy	(mg/cc)	1.56±0.20			2.02±0.30		
Cancer	NIC	0.09±0.01	8.486	0.000	0.40±0.05	14.768	0.000
Healthy		0.02±0.002			0.06±0.004		
Cancer	λ_{HU}	1.87±0.25	9.273	0.000	2.89±0.41	15.095	0.000
Healthy		0.51±0.05			0.50±0.03		

[Downloaded from ijrr.com on 2026-11-12]

[DOI: 10.52547/ijrr.20.2.5]

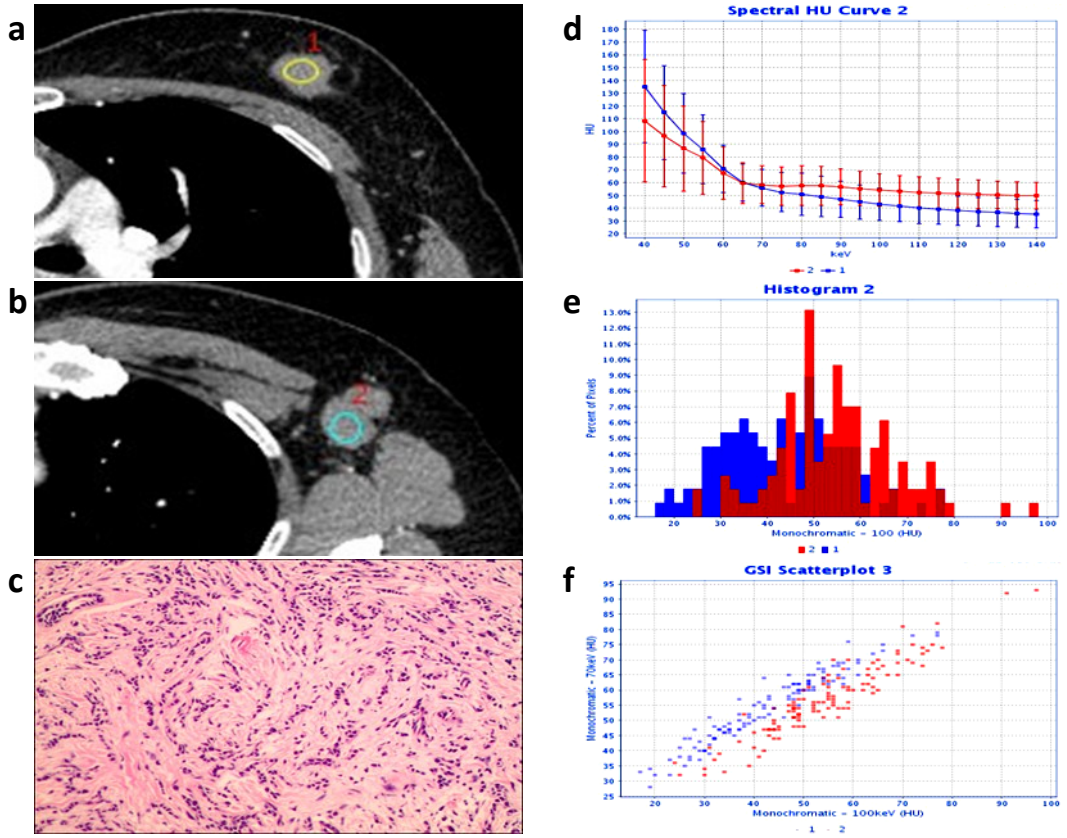


Figure 5. Arterial phase monochromatic images at 65keV in GSI mode in a 40-year-old woman presenting invasive ductal carcinoma **(a)** and metastatic axillary lymph node **(b)** established by pathology **(c)** (HE: ×100). The spectral curve **(d)**, histogram **(e)**, and scatter plot **(f)** of cancerous breast tissue and metastatic lymph node were crossed in the arterial phase.

Table 5. Comparison of radiation dose parameters of spectral CT and traditional chest dual-phase enhanced CT.

N	CTDIvol (mGy)		DLP (mGy-cm)/phase		ED (mSv)/phase	
	Traditional CT	Spectral CT	Traditional CT	Spectral CT	Traditional CT	Spectral CT
1	11.85	7.64	320.18	252.59	4.48	3.53
2	16.48	7.64	572.20	257.94	8.01	3.61
3	16.36	7.64	476.28	247.24	6.66	3.46
4	16.58	7.64	691.76	241.89	9.68	3.38
5	16.44	7.64	536.28	279.34	7.50	3.91
6	10.10	7.64	368.80	284.70	5.16	3.98
7	16.48	7.64	583.47	279.34	8.16	3.91
8	16.49	7.64	584.02	247.24	8.17	3.46
9	13.33	7.64	506.23	322.15	7.08	4.51
10	11.85	7.64	320.18	300.75	4.48	4.21
11	11.37	7.64	307.17	257.94	4.30	3.61
12	9.50	7.64	326.00	278.35	4.56	3.89
`x±s	13.90±2.83	7.64±0.00	466.05±132.6	270.79±24.37	6.52±1.85	3.79±0.34
t	-		-		5.016	
p-Value	-		-		0.000	

DISCUSSION

In oncological imaging, spectral CT has promising clinical applications for the characterization of tumors [11, 12]. Due to the breast cancer lesions have a richer blood supply and denser cancer cells than normal breast glands, the CT values between 40keV and 140keV, λ_{HU}, and IC or NIC of breast cancer were higher than normal breast tissue in the plain, arterial and venous phases, it was more useful for preoperative breast cancer detection when compared with traditional CT, the specific advantages of dual-energy CT and mechanisms are discussed as follows.

Because of the energy dependence of X-ray attenuation, image noise and contrast decrease with the increase in keV [13], a balance between image noise and contrast will be achieved when an appropriate keV is selected, thereby obtaining images with the optimal CNR. Monochromatic levels that showed specific tissues or lesions with an optimal CNR were obtained using the optimal CNR monochromatic curve. Our study indicated that the monochromatic level that showed normal breast

[Downloaded from ijrr.com on 2026-11-12]

[DOI: 10.52547/ijrr.20.2.5]

tissue with optimal CNR was approximately 65keV in the plain, arterial, and venous phases. At this energy level, excellent image contrast was maintained, while the image noise was simultaneously reduced.

Conventional CT cannot offer absolute values and effectively reflect the material density, mainly due to its polychromatic X-ray beams [14]. In contrast, spectral CT can create 101 monochromatic images between 40keV and 140keV, and the differences between tissues in monochromatic images are mainly determined by their density. Therefore, there is a one-to-one correspondence between CT value and tissue density, and the CT values are more accurate and reflect the tissue differences reliably than traditional CT [15]. CT values between 40keV and 140keV were represented by the spectral curve, and the same tissue or pathological structures had similar λ_{HU} values, which can provide quantitative information about tissue composition and have been shown to be able to differentiate diagnoses [16].

The detection of lesions in traditional CT imaging mainly relies on the gray differences before and after enhancement, but the result is easily influenced by the CT values of the background tissue and partial volume effect; therefore, a slight discrepancy in IC would not be recognized. Slight differences in IC in iodine-based material images could induce obvious gray discrepancies and sensitively reflect the lesion's true IC value because iodine-based material images can limit the influence of background tissue CT values and partial volume effects more than traditional CT images [17, 18]. Studies have found that the boundary between tumors and the surrounding normal tissues has been unclear in polychromatic images from traditional CT, while iodine-based material images were able to clearly show the tumor extension and the relationship between the lesion and surrounding great vessels [19]. A previous study [20] showed that vasculature remodeling or neoangiogenesis is an initiating event in the early stage of tumor development; iodine distribution in the tissue is strongly related to local blood volume and vascular density. Therefore, NIC may be used as a surrogate imaging marker for assessing angiogenesis in breast cancer [21]. Studies have shown that there is no statistical significance between the measured iodine content and the true value [22]. It has also been reported that the two-material decomposition technique can obtain accurate iodine content measurements [23]. Meng *et al.* [24] observed that healthy gastric mucosa had a lower IC than the mucosa in gastric carcinomas in iodine-mapping images by spectral CT; this observation could help differentiate images of pathologic and normal tissues.

The axillary lymph nodes are the most common site for breast cancer, and correct identification is important for both determining the patient's prognosis and planning treatment [25]. Lymph node status assessments with traditional CT are mainly based on the size, margin, number, CT values, and enhanced types, which cannot accurately predict the status of lymph nodes and produce false results [26]. All or part of the normal structure of metastatic lymph nodes is replaced or destroyed by the invading tumor cells compared with reactive lymph node hyperplasia, so the metastatic lymph nodes show similar microstructure and biological behavior to the primary lesions. Analyzing the spectral features, such as the morphology, histogram, and scatter plot distribution of metastatic lymph nodes and primary lesions, can be helpful for the differentiation and qualitative diagnosis of lymphadenopathy [27-29]. A recent study [21] demonstrated that λ_{Hu} was the single best parameter for the detection of metastatic sentinel lymph nodes in breast cancer, and our study showed that metastatic lymph nodes had nearly the same spectral curve, histogram, and scatter plot morphology as breast cancer primary lesions in the venous phase. The graphs were different or crossed in the arterial phase, which is consistent with the finding of a previous study [30], which showed that venous phase λ_{Hu} was the most helpful parameter to diagnose metastatic lymph nodes. The venous phase λ_{Hu} accurately detected 90.5% of metastatic lymph nodes among all lymph nodes analyzed, with an 87% accuracy among all patients analyzed, and the specificity and accuracy of the venous phase λ_{Hu} were higher than those obtained from the morphological parameters.

It is important to reduce the dose of radiation administered to female patients because the breast is sensitive to X-rays. According to this research, the radiation dose of spectral CT for dual-phase scanning was lower than that of traditional CT scanning. This is mainly due to the application of new scanning technology with fast switching between 80 kVp and 140 kVp and adaptive statistical iterative reconstruction technology.

CONCLUSION

In conclusion, spectral CT not only reduces the radiation dose, but it also provides high-quality images and multiple quantitative parameters. These parameters are complementary to conventional CT and improve the detection and assessment of cancerous breast tissue and metastatic lymph nodes. Spectral CT further improves the limitations of traditional CT in breast examination, providing more reliable information and methods for clinicians.

Ethical approval

All measurements from human subjects were obtained in full ethical accordance with both the local institutional research committee and the 1964 Helsinki Declaration. (Reference Number: 2020 14; Date: 2020-05-08.

[Downloaded from ijrr.com on 2026-11-12]

[DOI: 10.52547/ijrr.20.2.5]

ACKNOWLEDGEMENTS

Thanks to Xinyue Yang, an economics major at Miami University, for the English translation and editing.

***Conflicts of interest*:** None declared.
***Funding*:** The Medical Health Science and Technology Project of Zhejiang Provincial Health Commission (Grant no. 2020KY1050).
***Ethical consideration*:** This study was approved by the Taizhou Central Hospital ethics committee.
***Author contributions*:** (L.J.Ch) designed experiments; (B.W) and (S.F.W) carried out experiments; (L.J.Ch), (Z.L. X), (L.Z.J) and (M.H.H) analyzed experimental results; (L.J.Ch) and (X.P.Y) and (G.Y. W) wrote the manuscript.

REFERENCES

1. Torre LA, Bray F, Siegel RL, Ferlay J, Lortet-Tieulent J, Jemal A (2015) Global cancer statistics, 2012. *CA Cancer J Clin, **65**: 87–108*.
2. Casiraghi M, De Pas T, Maisonneuve P (2011) A 10-year single-center experience on 708 lung metastasectomies: the evidence of the "international registry of lung metastases". *J Thorac Oncol, **6**: 1373–1378*.
3. Mahner S, Schirrmacher S, Brenner W (2008) Comparison between positron emission tomography using 2-[fluorine-18] fluoro-2-deoxy-D-glucose, conventional imaging and computed tomography for staging of breast cancer. *Ann Oncol, **19**: 1249–1254*.
4. Zhao LQ, He W, Li JY (2012) Improving image quality in portal venography with spectral CT imaging. *Eur J Radiol, **81**: 1677-1681*.
5. Onishi S, Fujioka C, Kaichi Y (2019) Utility of dual-energy CT for predicting the vascularity of meningiomas. *Eur J Radiol, 123*.
6. Li M, Zhang L, Tang W (2019) Quantitative features of dual-energy spectral computed tomography for solid lung adenocarcinoma with EGFR and KRAS mutations, and ALK rearrangement: a preliminary study. *Transl Lung Cancer Res, **8**: 401–412*.
7. Kaltenbach B, Wichmann JL, Pfeifer S (2018) Iodine quantification to distinguish hepatic neuroendocrine tumor metastasis from hepatocellular carcinoma at dual-source dual-energy liver CT. *Eur J Radiol, **105**: 20–24*.
8. Udare A, Walker D, Krishna S (2020) Characterization of clear cell renal cell carcinoma and other renal tumors: evaluation of dual-energy CT using material-specific iodine and fat imaging. *Eur Radiol, **30**: 2091–2102*.
9. Tawfik AM, Razek AA, Kerl JM, Nour-Eldin NE, Bauer R, Vogl TJ (2014) Comparison of dual-energy CT-derived iodine content and iodine overlay of normal, inflammatory and metastatic squamous cell carcinoma cervical lymph nodes. *Eur Radiol, **24**: 574–580*.
10. Metin Y, Metin NO, Ozdemir O, Tasci F, Kul S (2020) The role of low keV virtual monochromatic imaging in increasing the conspicuity of primary breast cancer in dual-energy spectral thoracic CT examination for staging purposes. *Acta Radiol, **61**: 168–174*.
11. Simons D, Kachelriess M, Schlemmer HP (2014) Recent developments of dual-energy CT in oncology. *Eur Radiol, **24**: 930-939*.
12. Zhang Y, Bai L, Wen Y, *et al.* (2021) Differential diagnosis of pancreatic cystic masses with the quantitative analysis of spectral CT imaging: Initial results. *Int J Radiat Res, **19**: 155-165*.
13. Lin XZ, Wu ZY, Tao R (2012) Dual energy spectral CT imaging of insulinoma-Value in preoperative diagnosis compared with conventional multi-detector CT. *Eur J Radiol, **81**: 2487-2494*.
14. Stolzmann P, Scheffel H, Rentsch K (2008) Dual-energy computed tomography for the differentiation of uric acid stones: ex vivo performance evaluation. *Urol Res, **36**: 133-138*.
15. Liu X, Yu L, Primak AN (2009) Quantitative imaging of element composition and mass fraction using dual- energy CT: Three-material decomposition. *Med Phys, **36**: 1602-1609*.
16. Boll DT, Patil NA, Paulson EK (2010) Focal cystic high-attenuation lesions: characterization in renal phantom by using photon counting spectral CT--improved differentiation of lesion composition. *Radiology, **254**: 270-276*.
17. Chae EJ, Song JW, Seo JB (2008) Clinical utility of dual-energy CT in the evaluation of solitary pulmonary nodules: initial experience. *Radiology, **249**: 671-681*.
18. Yeh BM, Shepherd JA, Wang ZJ. (2009) Dual-energy and low-kVp CT in the abdomen. *AJR Am J Roentgenol, **193**: 47-54*.
19. Zhou J and Lv YC (2011) The application of Computed Tomography Spectral Imaging in the Diagnosis of Tumors. *Chinese Journal of Neuro-oncology **9**: 263-266*.
20. Gao F, Li M, Ge X (2013) Multi-detector spiral CT study of the relationships between pulmonary ground-glass nodules and blood vessels. *Eur Radiol, **23**: 3271-7*.
21. Wang XX, Liu DH, Zeng XF (2021) Dual-energy CT quantitative parameters for the differentiation of benign from malignant lesions and the prediction of histopathological and molecular subtypes in breast cancer. *Quant Imaging Med Surg, **11**: 1946-1957*.
22. Zhang D, Li X, Liu B (2011) Objective characterization of GE discovery CT750 HD scanner: gemstone spectral imaging mode. *Med Phys, **38**: 1178-1188*.
23. Chen KM (2012) Applications of spectral CT imaging. Beijing: Science Press
24. Meng X, Ni C, Shen Y (2017) Differentiating malignant from benign gastric mucosal lesions with quantitative analysis in dual energy spectral computed tomography: Initial experience. *Medicine (Baltimore) **96**: e5878*.
25. Buus TW, Sandah M, Thorup KS (2021) Breast cancer: comparison of quantitative dual-layer spectral CT and axillary ultrasonography for preoperative diagnosis of metastatic axillary lymph nodes. *European Radiology Experimental, **5**: 16*.
26. Obwegeser R, Lorenz K, Hohlagschwandtner M (2000) Axillar y lymph nodes in breast cancer: Is size re lated to metastatic involvement. *World J Surg, **24**: 546-550*.
27. Lin XZ, Li WX, Zhu YB (2010) Preliminary application of Gemstone Spectral Imaging (GSI) in the diagnosis of tumors. *J Diagn Concepts Pract, **9**: 155-160*.
28. Matsumoto K, Jinzaki M, Tanami Y (2011) Virtual monochromatic spectral imaging with fast kilovoltage switching: improved image quality as compared with that obtained with conventional 120-kVp CT. *Radiology, **259**: 257-262*.
29. Ou Yang AM, Su XY, Wei ZL (2015) Application progresses of gemstone spectral imaging in the diagnosis and therapy of tumors. *J Chin Clin Med Imaging, **26**: 602-604*.
30. Zhang X, Zheng C, Yang Z (2018) Axillary Sentinel Lymph Nodes in Breast Cancer: Quantitative Evaluation at Dual-Energy CT. *Radiology, **289**: 337-346*.

[Downloaded from ijrr.com on 2026-11-12]

[DOI: 10.52547/ijrr.20.2.5]

[DOI: 10.52547/ijrr.20.2.5] [Downloaded from ijrr.com on 2026-11-12]